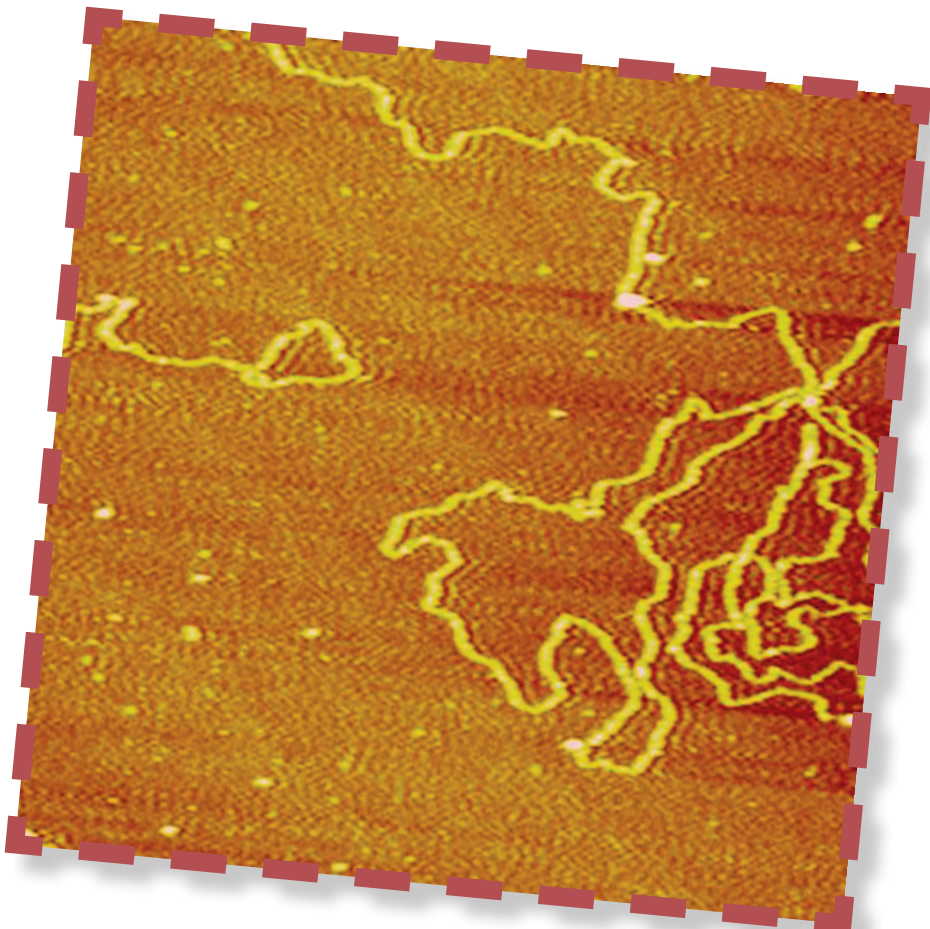


VALIDATION AND VERIFICATION OF IMAGES IN ATOMIC FORCE MICROSCOPY

SRINIVASA M. SALAPAKA,
ADITYA RAMAMOORTHY,
and MURTI V. SALAPAKA



AFM Imaging— Reliable or Not?

Atomic force microscopy (AFM) was invented in 1986 [1]. By using a compliant flexure probe, such as a microcantilever beam with a sharp tip at one end, the interaction forces between atoms on the probe-tip and atoms on the material surface can be measured (see Figure 1). Since its invention, the simple strategy of using a beam with a sharp tip is now being employed to measure many diverse properties of matter at the nanometer scale including electrical, magnetic, chemical, and mechanical properties [2]. Many different operational modes have evolved that have demonstrated the versatility of the basic underlying principle [3]. AFM has led to many seminal insights in science such as obtained in the recent imaging of pentacene molecules with subatomic resolution [4].

Feedback control has been at the heart of the AFM since its inception. Binnig and collaborators [1] realized that feedback can be employed to manage the difficulties posed by the complex dependency of forces that affect the separation between the tip and the material surface atoms. Over the past decade, systems and control researchers have made enabling contributions to increase the temporal and spatial resolutions possible with AFM [5]. While two-and-a-half decades have passed since the invention of AFM, during which many design refinements have been made, there is still ample scope for improving image resolution and bandwidth. This unrealized potential, together with high performance demands from a growing number of applications (such as video-rate imaging of cellular functions [6]), has spurred considerable research interest in device redesign and development of new modes of operation. In this context, there has been a surge in system theoretic analysis and design methods, which provide a systematic study of

Digital Object Identifier 10.1109/MCS.2013.2279475
Date of publication: 14 November 2013

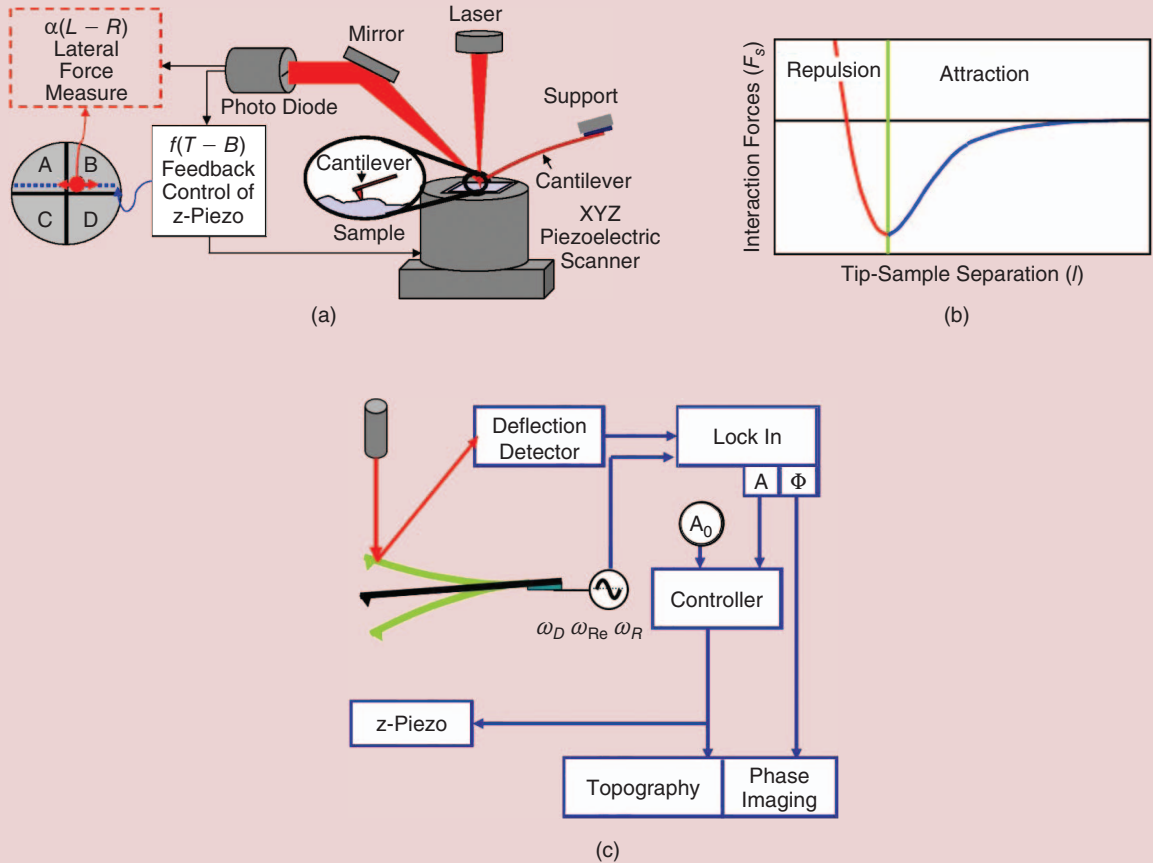


FIGURE 1 A schematic of an atomic force microscope and its modes of operation. (a) The main probe of an atomic force microscope is a microcantilever, which deflects due to interactive forces (10^{-12} – 10^{-7} N) between the atoms on the sample and the atoms on the tip. The deflection of the cantilever is registered by a laser incident on the cantilever, which reflects onto a photodiode split into four cells. The difference between the readings from the top and the bottom cells gives a measurement proportional to the cantilever's normal deflection. A piezo scanner positions the sample relative to the cantilever in the lateral and the vertical directions. A dither piezo actuator that lies under the cantilever support can be used to provide vertical motion to the cantilever. The difference between the readings from the left and the right cells, which gives a measurement proportional to the cantilever's twist angle, is regarded as a measure of lateral forces. (b) A representative profile of forces between the sample and the tip with long-range attractive and short-range strong repulsive forces. During a scan, the sample is moved laterally under the cantilever, and the image is derived from the cantilever deflections at each point of the lateral motion. Depending on the sample and intended applications, different imaging modes are used. For instance, in the *contact-mode operation*, the cantilever tip is maintained at a setpoint corresponding to a tip-sample force in the repulsive region. The control signal, which regulates a reference setpoint by moving the sample vertically relative to the cantilever probe, thereby compensating for the sample feature heights during the scan, gives a measure of the sample topography. This mode of operation is hard on the tip and the sample and can lead to wear on both [29]. However, this mode is simpler to analyze and implement than other schemes. In the dynamic mode, the cantilever is oscillated sinusoidally (by actuating the dither piezo) typically at or near its resonance frequency. In this method, the changes in the tip-sample interaction forces during a scan affect the oscillation attributes (such as amplitude, frequency, and phase), and these effects are used to map the sample topography [29], [30]. However, because of the intermittent contact with the sample, the lateral drag forces are substantially reduced, making it possible to image soft material that is not possible with the contact-mode operation. (c) The diagram depicts the amplitude-modulation mode, a dynamic mode of operation where the oscillation amplitude is regulated at a setpoint. In this mode too, the control signal required for amplitude regulation gives a measure of the sample topography.

underlying principles and fundamental limitations, and develop control designs that improve imaging resolution, bandwidth, and reliability of atomic force microscopes.

AFM operation can be fraught with subtle effects [3]. Discerning these effects is currently limited to experienced AFM researchers. Atomic force microscopes are used by a wide diversity of researchers with backgrounds in disparate areas such as biology and material science. In light of

its widespread usage in diverse areas where many users are not experts in AFM, it is important to quantify the quality of AFM-based images. Currently, there is a lack of measures that enable assessment of AFM image quality. There is an urgent need for approaches that i) eliminate spurious effects from AFM operation, ii) provide fidelity measures on images that are real-time implementable, and are iii) easy to interpret.

AFM has led to many seminal insights in science such as obtained in the recent imaging of pentacene molecules with subatomic resolution.

There are considerable challenges in addressing the need for effective methods for minimizing artifacts in AFM-based imaging and the associated task of providing fidelity measures on the quality of the image acquired. Spurious data arise from the deviation of device design from its intended purpose, lack of understanding of device limitations, and inaccurate assumptions about AFM operation that lead to misinterpretation of data. For instance, the laser-optics geometry may not be aligned as intended, the shape of the cantilever tip may disallow profiling of sharp corners, compliance of the sample may be ignored as is typically done in many imaging modes, or the irregularities of tip-sample force regulation may be ignored thereby leading to a misinterpretation of the image. Deciphering and isolating these different sources of incorrect inferences remains a formidable task.

Moreover, the recent emphasis on high-bandwidth and high-resolution imaging has led to an increase in complexity in many operational modes of AFM imaging. In particular, there is considerable emphasis on the dynamic-mode operation, which is considerably gentler than the originally envisioned contact-mode operation. In many applications, particularly involving soft matter, it is the only mode of AFM operation used [3]. In this mode, in addition to the tip-sample interaction forces, the cantilever is also subjected to an external sinusoidal forcing. Properties of the sample are derived by monitoring the oscillations of the cantilever. The resulting dynamics are not only nonlinear but also time varying. Furthermore, the need for high bandwidth with high resolution necessitates methods for addressing the spillover of effects encountered by the cantilever in the past on the feature being explored currently. The difficulty is further compounded because the cantilever oscillations are dependent on tip-sample interaction forces. Thus, it becomes important to understand how the sample property of interest alters the tip-sample interaction force. Here feedback strategies can prove crucial [5]; however, feedback and the associated hardware introduce their own dynamics, limitations, and imaging artifacts [7], [8]. These sources of complexity and uncertainty in AFM-based imaging can result in significant misinterpretation of data.

This article presents initial steps for a framework for how control and information theoretic concepts can be used to reduce spuriousness in AFM-based imaging and provide quality measures on AFM images. These concepts are presented via two specific application contexts. The first part analyzes some sources of artifacts in high-resolution

(nanometer to subnanometer) contact-mode AFM imaging and provides feedback-based strategies to minimize these effects. In the second part, a high-bandwidth, dynamic-mode, sample-feature detection method is presented, where high-bandwidth and high-resolution needs motivate methods to discern and remove undesirable effects caused by complex nonlinear dynamics. These two contexts are illustrative and should not be considered as being comprehensive. A control systems perspective is shown to enable a framework for providing quantitative measures of image fidelity in real time.

HIGH-RESOLUTION CONTACT-MODE IMAGING

Typical artifacts in high-resolution (subnanometer) AFM imaging are mainly caused by geometric cross talk, tip-sample stick, mechanical cross talk, piezo drift and creep, tip-sample convolution, and thermal and electronic noise. This article focuses on the first three causes of artifacts. Classes of artifacts not emphasized in this article are described in [5] and [9]–[12], which illustrate how robust control tools can be employed to address their effects. *Geometric cross talk* refers to cross-coupling between the vertical and lateral cantilever deflections, leading to incorrect inferences on the normal and lateral forces felt by the cantilever. The cause is misalignment between the laser path and cantilever axes due to fabrication inaccuracies, misalignments in photodiode-sensor-laser source assembly, and difficulties in correctly mounting the cantilever. The effects of geometric cross talk are shown in Figure 2, where plot (a) shows lateral and vertical measurements as the cantilever is brought close to the sample and then retracted vertically. The measured lateral deflection is proportional to the measured vertical deflection. Here, geometric cross talk results in a perception of a lateral deflection of the cantilever. The experiment in Figure 2(b) is identical to the experiment in (a) except that the cantilever was removed and manually mounted again, thereby altering the alignment from that in (a). The difference in lateral signals in the two experiments indicates that measurements are sensitive to misalignments in the laser path and cantilever axes.

In the constant-force contact mode of AFM operation, typically the vertical deflection of the cantilever is maintained at a desired setpoint, and the coupling of vertical motion to the lateral deflection measurement is small. However, lateral frictional forces lead to torsional forces on the cantilever resulting in lateral deflection measurements that can spill into the vertical deflection measurement due to geometric cross talk. Such spuriousness can be further compounded by another

prominent source of artifacts based on frictional forces caused by *tip-sample stick*, where frictional forces cause the tip to be stuck at a location, hindering the lateral motion of the cantilever tip with respect to the sample in a scan. Thus, the vertical deflection is interpreted as an incorrect lateral coordinate. These effects of lateral deflections spilling over to the vertical deflection measurements and effects of tip-sample stick are illustrated in Figure 3. This figure shows experimentally measured lateral and vertical forces from imaging mica, which has a characteristic length of 5.2 Å. Here, as in many nanotribological investigations [13], the sample was moved laterally in a direction perpendicular to the cantilever axis. The large lateral deflections are the result of twisting the cantilever. The

height signal, which characterizes the height of the topography, is expected to be small (approximately few angstroms) since the mica sample is atomically flat. However, Figure 3(b) shows a height signal that is not small but is proportional to the lateral signal [shown in Figure 3(a)], indicating geometric cross talk. The linear portion of the waveform (with low slope) in the lateral force measurements in Figure 3(c) corresponds the cantilever being *stuck* to the mica surface, with the cantilever twist increasing linearly. The sudden fall (the linear portion with high slope) corresponds to cantilever *slip*, where the cantilever suddenly starts sliding when its restoring forces overcome the lateral friction forces. Thus, for an apparent travel range of about 5.2 Å, which is close to the lattice dimension of mica, the tip is stuck to a single location and the corresponding height signal during this stick regime represents the height of the stuck location rather than the intended locations along the scan line. During tip-sample stick, the height image is expected to be flat since it represents the height data at *a fixed location*. However, due to the geometrical cross talk, a spurious linear trend is seen in the vertical deflection (height) data.

Mechanical cross talk refers to spurious measurements of vertical deflection caused by lateral interaction forces between the cantilever tip and the sample surface that excite the buckling

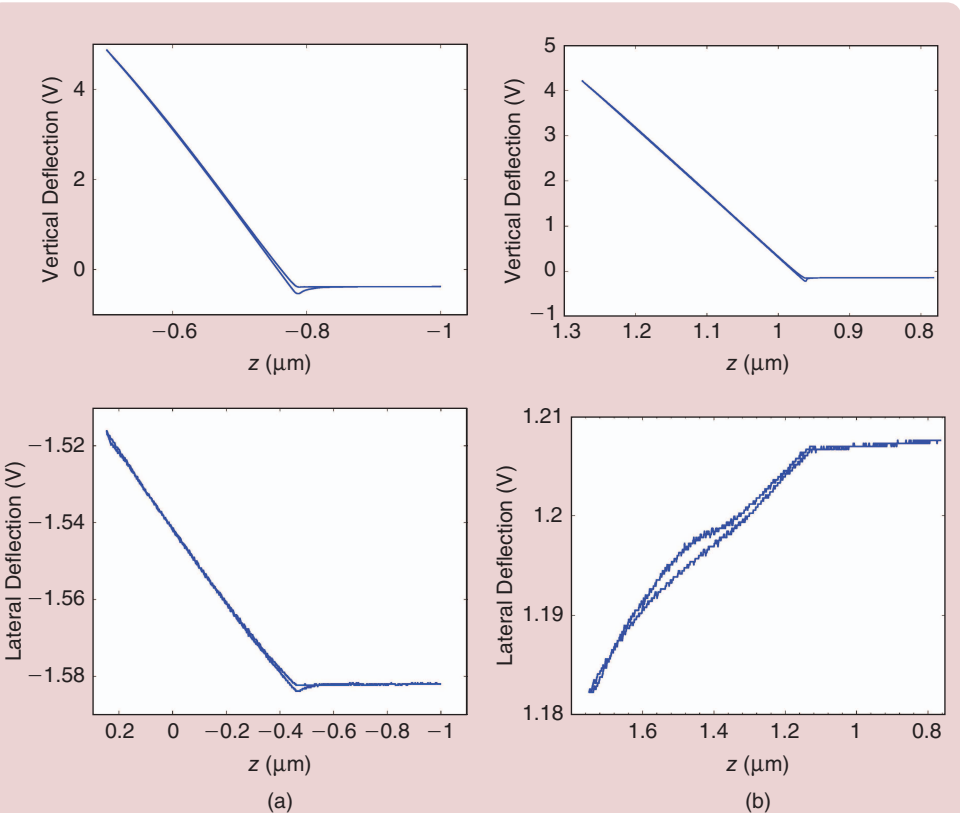


FIGURE 2 Effects of geometric cross talk in vertical/lateral displacement experiments. Both (a) and (b) show the vertical and lateral deflection signals from the photodiode sensor of the atomic force microscope as the cantilever tip is brought close to and then retracted away from the sample. The cantilever alignment with respect to the optical assembly in (a) is different from that in (b).

and twisting dynamics of the cantilever. Spurious vertical deflection measurements can result even in the absence of geometric cross talk. Both buckling and vertical deflection change the slope of the reflecting surface of the cantilever, leading to a change in the reflected laser beam, and hence are indistinguishable to the photodiode sensor [see Figure 4(a)]. Similarly, when the cantilever twists by large angles, the lateral rotation of the reflecting surface of the cantilever not only deflects the laser beam in the lateral direction but also in the vertical direction [see Figure 4(b)]. Mechanical cross talk only affects measurement of the vertical deflections and not the lateral measurements since vertical deflections and buckling do not create twisting effects. The artifacts are more pronounced when sample features are very small and have significant friction variation.

In [14], a solution is presented to *simultaneously* correct in real time both the geometrical and mechanical cross talk. The problem of tip-sample stick is also resolved. Here both *vertical* and *lateral* cantilever deflections, as measured by the photodiode, are regulated to constant setpoints through feedback (see Figure 5). The basis of this solution lies in the fact that both forms of cross talk and tip-sample stick result in spurious signals in one channel only when there is a variation of the cantilever deflection in the other direction. In existing AFM setups,

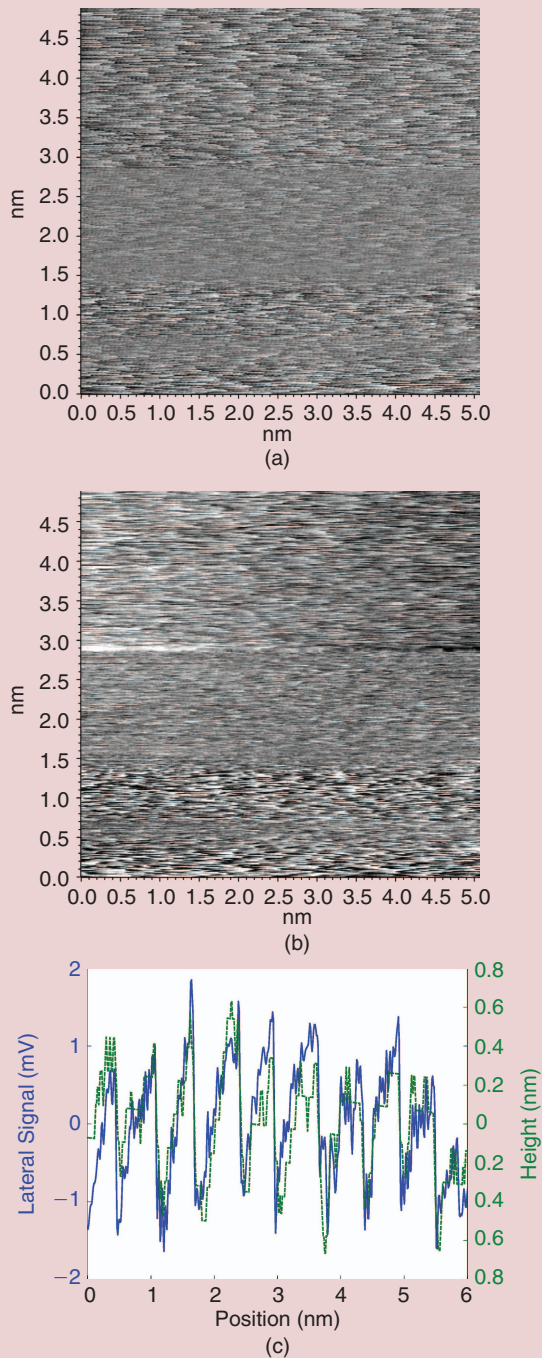


FIGURE 3 Effects of geometric cross talk and tip-sample stick-slip in a high-resolution image of mica. (a) Lateral-force image of mica obtained by plotting lateral deflection of the cantilever as a function of its position on the mica sample. The fuzziness indicates lattice-scale stick slip [13], [31]. (b) Topographical-height image of mica obtained by plotting the vertical deflection of the cantilever as a function of its position. The fuzziness similar to that in (a) is an artifact since features with atomic-scale heights are expected. (c) Topographical-height and lateral-force images when superimposed from the same scan line obtained from the images (a) and (b) shows very high correlation between the two.

actuators and feedback-related hardware are present for regulating a desired constant cantilever deflection. Typically at normal operating conditions, the feedback is effective in maintaining vertical deflection close to the desired setpoint and the spillover of vertical deflection into measurements of lateral deflection is small. Likewise, [14] reports an actuator design and a feedback scheme that regulates the lateral deflection at a constant value. To enable a lateral compensation feedback scheme, the cantilever holder in the atomic force microscope (molecular force probe 3D (MFP-3D) from Asylum Research Inc., Santa Barbara) was modified to incorporate a rudimentary lateral actuator. The existing high-frequency dither piezo at the base of the cantilever clamp was replaced with a set of split piezos, each of which is actuated by voltage inputs that are 180° out of phase. As a consequence, the piezos move 180° out of phase with each other. When one piezo expands, the other contracts to create a rotational effect on the cantilever clamp. This rotation of the cantilever clamp has the effect of laterally rotating the free end of the cantilever reflective surface. The split piezo assembly rotates the whole cantilever along with its substrate, thereby providing control over the twist of the cantilever. The feedback law in [14] was a proportional-integral controller that regulated the difference between the reference setpoint and the sensor reading (lateral signal from the quadrant photodiode) to zero.

The dual feedback scheme renders the measurements insensitive to the misalignment of the axes on the photodiode sensor with respect to the cantilever axes (see Figure 6). When the lateral control is switched off, the lateral deflection measurements in (a) indicate stick-slip motion. The corresponding vertical (feature-height) signal shown in (b) exhibits its geometric cross talk, where the height signal is expected to be atomically flat but is proportional to the lateral signal. The trace and retrace height signals, which are supposed to overlap, have a difference of 1.489 nm. When control is activated, the lateral deflection is regulated [shown in (c)] and does not show any stick-slip effects. Due to regulation of lateral twisting, the geometric cross talk is practically eliminated, and the trace and retrace overlap each other, as seen in (d). The difference between the height trace and retrace with the lateral position under feedback compensation is 0.288 nm, which is within the z-resolution value for the contact-mode operation. The above solution exemplifies the case where a new operational mode, facilitated by feedback, is developed to make measurements insensitive to inaccuracies due to fabrication and assembly errors.

High-Bandwidth Dynamic-Mode Detection

The previous section illustrated artifacts in AFM images obtained in the contact-mode operation. While many similar issues are present in the *dynamic-mode* operation of an atomic force microscope, here, a major source of misinterpretation of measured data is the increased complexity of

This article presents initial steps for a framework for how control and information theoretic concepts can be used to reduce spuriousness in AFM-based imaging and provide quality measures on AFM images.

the dynamics. The increased complexity is caused by the large oscillations of the cantilever, where a large range of tip-sample nonlinear interaction is explored, coupled with external forcing that makes the dynamics time-varying.

As discussed earlier, there is little current emphasis on methods that provide quantitative metrics on the image fidelity. Developing a general approach for providing fidelity measures is challenging in general, and related research is in its infancy. The beginnings of such a framework are being developed for the easier scenario where one material feature has to be distinguished from another. The aim is to *detect* the presence or absence of sample features, where obtaining more detailed information, such as the height of features, is not essential. For example, in a read operation in a data storage application, distinguishing a high-topographic profile encoding a one from a low-topographic profile encoding a zero is important [15], [16] but an exact measurement of the height is not required. Note that it is possible to increase the areal density by encoding multiple bits at the same location using different heights in topography to indicate different bits. For example, in [17] high areal density is enabled by encoding multiple levels in the height of the topographic features. Here the problem becomes detection of the height level rather than a simple detection of presence or absence of the sample.

Detection of features with high-temporal resolution is also motivated by studies that require real-time tracking of material deformation. For instance, in tracking biological motors and their motion, the location of the motor has to be detected [6]. Another example is the detection of changes in the sample properties, which is often the primary objective in material studies that investigate the effect of changes in environmental or control parameters (such as temperature or humidity) [3]. For these applications, where detection is more important, it is possible to envision methods that are not limited by the bandwidth of the positioning devices and the controller hardware. However,

to obtain high-speed detection, it is imperative to address the time scales of the cantilever dynamics.

As shown later, the lesser complexity of the detection task when compared to the task of obtaining more detailed information on the sample in a typical imaging scenario also facilitates quantitative measures on fidelity of detection schemes.

This article uses the example of a data-storage application to illustrate the beginnings of a machinery that can be employed to provide fidelity measures on probe-based

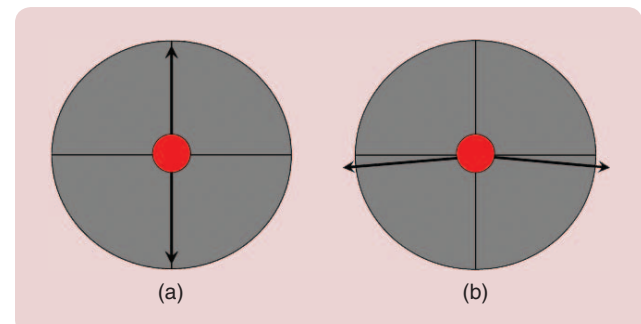


FIGURE 4 Effects of mechanical cross talk on the position of the laser spot. (a) The laser spot moves in the vertical direction when the cantilever buckles or deflects in the vertical direction, thus making it difficult to discern vertical deflection and buckling from each other. (b) When the cantilever twists under the influence of a lateral interaction force, the spot moves at an angle from the lateral axis.

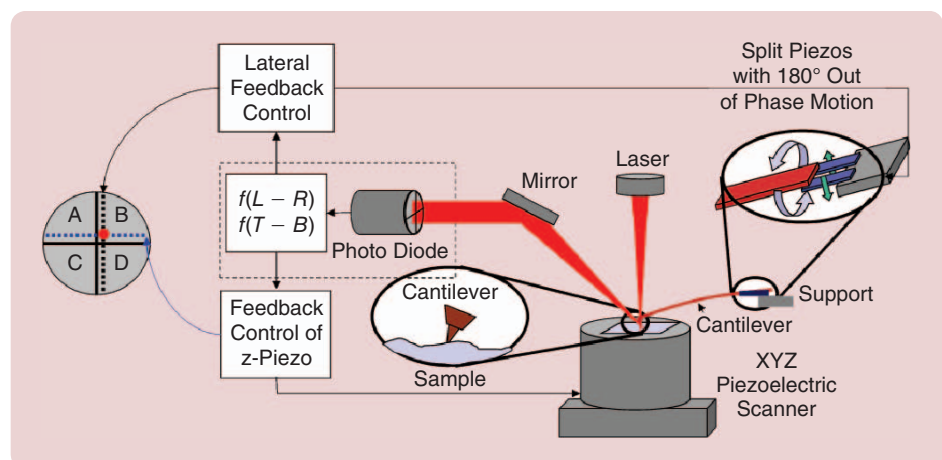


FIGURE 5 A schematic of the actuator design for lateral-force regulation. Two split piezos oscillating out of phase are used for lateral actuation (that is, to provide cantilever twist). A feedback controller uses lateral-force measurements to regulate the lateral forces on the cantilever.

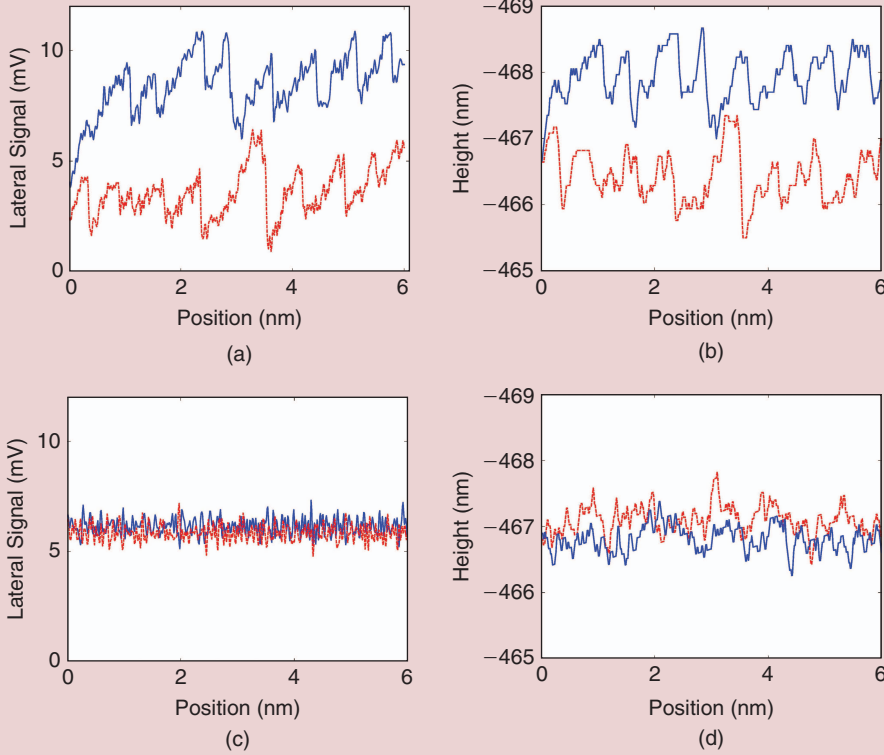


FIGURE 6 The effect of feedback-based regulation of lateral forces. (a) Lateral and (b) vertical trace and retrace measurements when the lateral-force regulation controller is switched off. (c) Lateral and (d) vertical trace and retrace measurements when the lateral-force regulation controller is switched on.

imaging. Here, the media or the sample being imaged is designed to store bits, where a sample feature with a particular topography encodes a “1,” and with another topography encodes a “0.” The discussion is limited to the detection of bits in the dynamic-mode operation of the atomic force microscope since it causes negligible damage to the tip and the media being interrogated (see Figure 1). Note that control systems, communication systems, and information-theoretic tools have played an important role in evaluating fidelity with which information can be retrieved in the contact-mode operation in a data-storage setting [18].

A key system-theoretic perspective that enables many significant insights for the dynamic mode is the Lure-feedback model of the cantilever dynamics [19], [20]. Figure 7 depicts this model. The cantilever is modeled as a linear time-invariant system G , with input being the sum of tip-sample interaction force h , the external dither excitation g (typically sinusoidal with frequency near the resonant frequency of the cantilever), and the thermal noise η , and the output being the cantilever deflection p . The noise introduced by the sensor in measuring the cantilever deflection is denoted by v , and the measured deflection is represented by y . The tip-sample interaction force is dependent on the cantilever position p and topography z . The tip-sample interaction model Φ in the feedback path of the Lure interconnection thus processes the

cantilever deflection to provide a force h on the cantilever.

The nonlinearity Φ in the feedback path is not known. However, an important observation that leads to a tractable model for feature detection is that the amplitude of cantilever oscillations are far larger than the effective range of the tip-sample interaction. Thus, the cantilever tip spends only a small fraction of its orbit under the sample’s influence. The short duration and intermittent interaction of the tip with the sample facilitates its modeling as an impulsive force on the cantilever tip. This model significantly simplifies the feature detection problem as it becomes equivalent to the detection of the *state-reset*—a sudden change in the state of the cantilever

due to an impulsive force. Thus the complexity of a nonlinearity in the feedback path is replaced by a model of the sample forces as a train of impulses with unknown strength. That is, the interaction force, $h(t)$ in Figure 7, is modeled as $\sum_k v_k \delta(t - t_k)$, where v_k and t_k represent the impulse strength and time instant of the k th encounter with the sample. Detection of a train of impulsive interactions that appear as inputs (see Figure 8) to a linear system with process noise η and measurement noise v is a well-studied problem in the systems literature. The application of the literature to this problem has resulted in the transient force AFM (TfAFM) method [21], [22], which is described next.

TfAFM Methodology, Capabilities, and Challenges

In TfAFM, sample features are detected using an observer-based state estimation scheme (see Figure 8). A state-space representation of the cantilever G is given by $\dot{x}_c = Ax_c + Bu$, $y = Cx_c + v$, and $u = \eta + g + h$ (where interaction force $h(t) = \sum_k v_k \delta(t - t_k)$ and A, B , and C are given by

$$A = \begin{bmatrix} 0 & 1 \\ -\omega_0^2 & -\omega_0/Q \end{bmatrix}, \quad B = \begin{bmatrix} 0 \\ 1 \end{bmatrix}, \quad C = \begin{bmatrix} 1 & 0 \end{bmatrix}.$$

The associated observer and state estimation error dynamics are

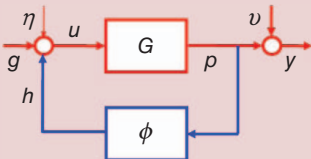


FIGURE 7 A Lure-feedback block diagram representation of the cantilever system in dynamic-mode imaging. The cantilever is modeled by a linear system G and the tip-sample interaction by a nonlinear map Φ . Here h , g , and η , respectively, represent the tip-sample interaction force, the dither forcing, and the thermal noise acting on the cantilever; and p , v , and y , respectively, represent the cantilever deflection, sensor noise, and the deflection measurement.

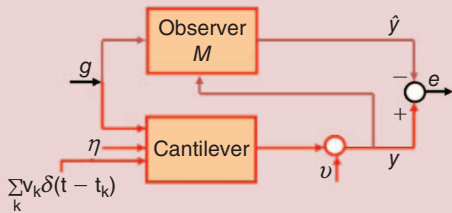


FIGURE 8 An observer architecture for the transient force atomic force microscopy imaging method. The influence of the sample is modeled as a train of impulses. Here η , g , v , and y are the thermal noise, external forcing, measurement noise, and measured cantilever deflection, respectively, and \hat{y} and e are the estimated deflection and error in estimation. The transfer function from the input to the cantilever to e and the impulse response can be analytically obtained. An impulse-response profile appears in e every time an impulsive force interaction occurs at the cantilever.

$$\begin{aligned} \dot{\hat{x}}_c &= A\hat{x}_c + Bg + L(y - \hat{y}), \\ \hat{y} &= C\hat{x}_c, \\ \text{State Estimation Error Dynamics} \\ \dot{\tilde{x}}_c &= Ax_c + B(g + \eta + h) - A\hat{x}_c - Bg - L(y - \hat{y}), \\ &= (A - LC)\tilde{x}_c + B\eta + B\sum_k \nu_k \delta(t - t_k) - Lv, \\ \tilde{x}_c(0) &= x_c(0) - \hat{x}_c(0), \end{aligned}$$

where L is the gain of the observer, \hat{x}_c is the estimate of the state x_c , and g is the known dither forcing applied to the cantilever. The error in the estimate is given by $\tilde{x}_c = x_c - \hat{x}_c$, and the error in the estimate of the output y is given by $e = y - \hat{y} = C\tilde{x}_c + v$.

In the above observer-based scheme, the decay rate of the state-estimation error \tilde{x}_c after encountering a feature (that leads to the state being reset to a new value) is decided by eigenvalues of $A - LC$. For AFM systems, the measurement noise is remarkably low, which allows for considerable freedom in the choice of L and makes it possible to track the state of the cantilever within a couple of oscillation cycles. TfAFM exploits this freedom for high-bandwidth imaging. Figure 9 shows images of DNA molecules whose height is in the 1.2–1.4 nm range. The TfAFM image,

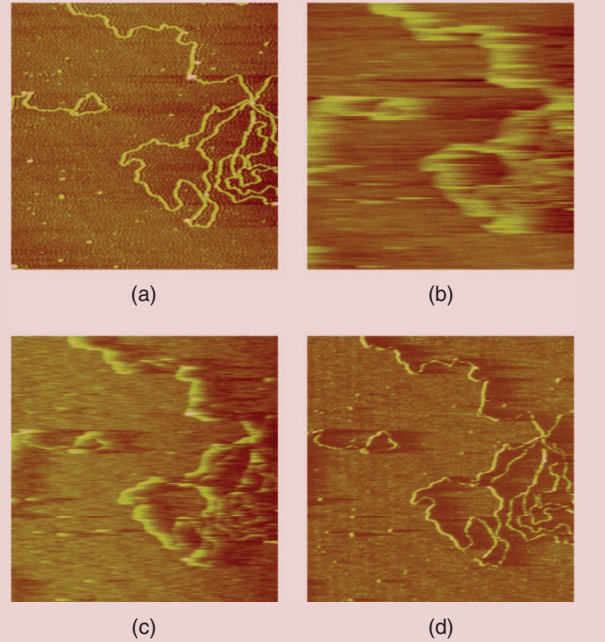


FIGURE 9 Real-time experimental data of dynamic-mode operation. (a) Height image of DNA at a normal scanning speed of 2 Hz, which is considered to be the true image. (b) Height image of DNA at a scan speed of 12 Hz. (c) Amplitude image of DNA at a scan speed of 12 Hz. (d) Transient force atomic force microscopy image of DNA at a scan speed of 12 Hz.

where the estimation error is plotted, is significantly better than the amplitude- (with respect to the first harmonic of the drive) and height- (the control signal) based images. This difference is due to the faster dynamics of the estimation error compared to the other variables. The amplitude, phase, height, and TfAFM images are obtained simultaneously in real time (phase images that show similar quality to the amplitude image are not shown).

Measures on Fidelity

Though important, confidence measures on AFM images are typically not specified. A framework to assess the fidelity of detection for the TfAFM method is developed below. The framework is explained in terms of the discretized model of the cantilever dynamics,

$$\begin{aligned} x_{k+1} &= Fx_k + G(g_k + \eta_k) + \delta_{\theta,k+1}v, \\ y_k &= Hx_k + v_k, \quad k \geq 0, \end{aligned} \quad (1)$$

where the matrices F , G , and H are obtained from matrices A , B , and C using a zero-order hold at a desired sampling frequency, $\delta_{i,j}$ denotes the Dirac delta function, θ denotes the time instant of the impact between the cantilever tip and the media, and v signifies the magnitude of the impact [22]. The impact results in an instantaneous change or jump in the state by v at time instant θ . Since in

While two-and-a-half decades have passed since the invention of AFM, during which many design refinements have been made, there is still ample scope for improving image resolution and bandwidth.

TfAFM, the map from the input forces on the cantilever to the error signal e (see Figure 8) is linear and time invariant, the error-signal profile can be precalculated as

$$e_k = y_k - \hat{y}_k = \Gamma_{k;\theta} \nu + n_k, \quad (2)$$

where $\{\Gamma_{k;\theta} \nu\}$ is a known dynamic-state profile with an unknown arrival time θ , $\Gamma_{k;\theta} = H(F - L_K H)^{k-\theta}$ for $k \geq \theta$ is the impulse response, L_K is the Kalman observer gain, and n_k is a zero-mean white noise sequence, which is the measurement residual had the impact not occurred. The statistics of n are given by

$$E\{n_j n_k^T\} = V \delta_{jk},$$

where $V = HP_{\tilde{\gamma}}H^T + R$ and $P_{\tilde{\gamma}}$ is the steady-state error covariance obtained from the Kalman filter [22].

Thus, determining whether or not the cantilever is interacting with the sample is equivalent to determining if the

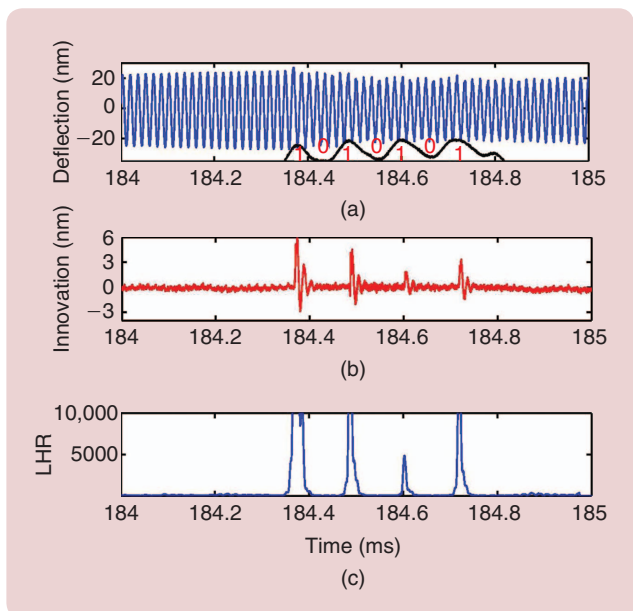


FIGURE 10 Transient force atomic force microscopy for data-storage systems. (a) The cantilever trajectory and a sample profile that encodes 1010101. (b) The innovation signal. (c) The likelihood ratio (LHR). Even though the second and third bits have the same topographic profiles, their signatures in the innovation signal are different with the 1 bit at 184.6 ms registering a smaller magnitude than the other bits.

dynamic profile is present or not. The innovation process e can be windowed into M samples depending on the effective length of the dynamic profile (characterized by $\Gamma_{k;\theta}$) followed by a hypothesis-testing step. The binary hypothesis-testing problem is

$$\begin{aligned} H_0 : e_k &= \gamma_k, & k = 1, 2, \dots, M, \\ \text{versus} \\ H_1 : e_k &= \Gamma_{k;\theta} \nu + n_k, & k = 1, 2, \dots, M, \end{aligned} \quad (3)$$

where $e_k = \gamma_k$ is the observed innovation and $\{\Gamma_{k;\theta} \nu\}$ for $k = 1, 2, \dots, M$ is a known *dynamic profile* with unknown arrival time θ and unknown magnitude of the state jump ν . For simplicity of exposition, it is assumed that the impact or state jump occurs at the first sample of each time window of M samples (that is $\theta = 1$). Thus,

$$\bar{e} = \Gamma \nu + \bar{n}, \quad (4)$$

where $\bar{e} = [e_1, e_2, \dots, e_M]^T$,

$$\Gamma = [H, H(F - L_K H), H(F - L_K H)^2, \dots, H(F - L_K H)^{M-1}]^T.$$

The likelihood ratio $l(\bar{e})$, which is the ratio $p(\bar{e}|H_1)/p(\bar{e}|H_0)$, can be compared with a threshold value as $l(\bar{e}) \gtrless_{H_0}^{H_1} \epsilon$ to arrive at a decision whether or not the dynamic profile is present. The threshold decides the desired fidelity of the detection and can be chosen to provide a suitable tradeoff between the rates of false detection and missed detection [23]. The false alarm P_F and detection probability P_D are given by

$$P_F = P_0(\Gamma) = \int_{\epsilon}^{\infty} p(l = L|H_0) dL$$

and

$$P_D(\nu) = P_1(\Gamma) = \int_{\epsilon}^{\infty} p(l = L|H_1, \nu) dL,$$

where $P_0(\Gamma)$ and $P_1(\Gamma)$, respectively, are the probabilities of detecting the dynamic profile Γ under hypothesis H_0 and H_1 and $p(l = L|H_0)$ and $p(l = L|H_1, \nu)$, respectively, are the probability density functions (pdfs) of likelihood ratio l under hypothesis H_0 and H_1 with state jump ν , respectively. Since $l = -(1/2) \sum_{i=1}^M e_i^T V^{-1} e_i$ under hypothesis H_0 , the function $p(l = L|H_0)$ is Chi-squared (χ^2) density with

M degrees of freedom. Similarly $l = -(1/2) \sum_{i=1}^M e_i^T V^{-1} e_i - (1/2) \nu \sum_{i=1}^M \Gamma_i^T V^{-1} e_i$ under hypothesis H_1 , $p(l=L|H_1)$ is a noncentral χ^2 density with noncentrality parameter $\nu^T (\Gamma^T \Gamma / V) \nu$. Thus for specified P_F (which does not depend on ν), the threshold ϵ can be computed from tables [24]. Given an estimate of the impulsive impact, P_D can be determined similarly.

In the above detection framework, it is possible to provide to the user control of the false alarm and detection probabilities. This capability can significantly enable researchers. For example, when the atomic force microscope is used to locate desired properties or features on the sample, the user could set the threshold ϵ to a low value, thereby detecting most of the features, albeit with the possibility of a large number of false positives. Such a low threshold value can be used to remove areas from further search where features are not detected. In subsequent iterations, the threshold could be increased to lower the false alarm rate and focus on the likely locations of features on the sample.

Figure 10 depicts experimental results that demonstrate the efficacy of TfAFM and the fidelity measures. In (a), the cantilever trajectory and the sample topography that simulate a data storage application are shown. There are four bits that encode the sequence 1010101, where the bit “1” is encoded as a hill and a valley represents a “0” bit. Note that it is difficult to discern the bits from the amplitude signal in (a). However, the bits are resolved in the innovation signal e , shown in (b). The likelihood ratio l is shown in (c). A threshold on the likelihood ratio can be used to decide whether the bit is a zero or not. For this experiment, if the threshold is over 5000, then it is possible that the high bit at 184.6 ms is wrongly classified as a zero. At a lower threshold, all four high bits are detected and correctly classified. Thus, by using the likelihood ratio (shown in Figure 10) and a threshold ϵ , the probability of false alarm and probability of detection can be provided, in addition to information on the bit detection.

A close observation of the experimental results in Figure 10(a) brings forth another issue—that the responses seen in the innovation signal to identical sample features (say “1” bits) are different. That is, the response at a feature depends not only on the feature but also on past features that the cantilever has encountered. This difference is explained by the fact that the cantilever is a force sensor. After the first encounter with the high-profile encoding a “1” at 184.4 ms, the amplitude of the cantilever oscillations decrease. Thus the cantilever interacts with the sample more gently when the high profile for the next “1” is encountered. The interaction with the third high profile is even gentler, leading to a smaller signature in the innovation signal. As the main purpose is to discriminate high-topographic profiles from low profiles, *memory* of the previous impacts leading to smaller oscillation amplitudes is a detriment. Given that the sample interaction is modeled

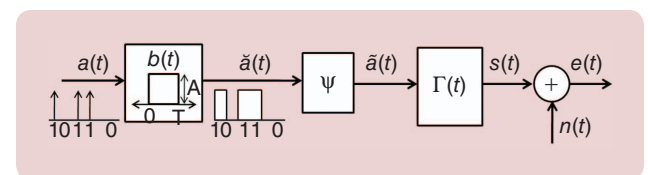


FIGURE 11 A continuous-time-channel model of a probe-based data storage system. In a data storage setting, the source sequence is encoded as a train of impulses [shown by $a(t)$]. Thus, the train is passed through a shaping filter $b(t)$ that results in the signal $\check{a}(t)$, which models the topography seen by the cantilever tip. The topography signal results in the force signal $\tilde{a}(t)$ to the cantilever. The force signal is a train of impulses where the impulse strength at a time instant can depend on the past topography. This dependence is characterized by Ψ . Γ is the impulse response from the input to the cantilever forcing to the innovation output $s(t)$. The innovation $e(t)$ incorporates the noise effects of noise $n(t)$ into $s(t)$.

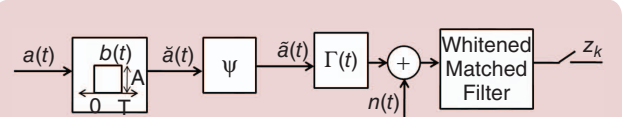


FIGURE 12 A discretized channel model with whitened matched filter [25].

as an impact, it is possible that the trajectory due to initial condition reset could be analytically deduced. However, results would become increasingly intractable with a large number of impulsive interactions to be considered, which is compounded by effect of noise.

In [25], an approach based on perspectives from communication systems is shown to address the *memory* issue. Figure 11 shows a communication-theoretic model of TfAFM. In this model, $\bar{a} = \{a_0, a_1, \dots\}$ with $a_i \in \{0, 1\}$ represents a string of bits encoded on the storage medium. Each bit is recorded on the medium with different topographic profiles encoding bits “0” and “1.” Since in AFM-based imaging the sample traverses under the cantilever, the sample topography can be viewed as a temporal signal encountered by the cantilever. Features corresponding to the string of bits \bar{a} on the storage medium can be viewed as temporal signal given by the convolution $\check{a}(t) = \sum_{k=0}^{N-1} a_k b(t - kT_c)$, where the impulse response $b(t)$ characterizes the bit profile. In this model, it is assumed that the cantilever samples (or encounters) the bit profiles at most $q = T/T_c$ times, where $T_c = 1/f_0$ is the oscillation frequency of the cantilever. As discussed in the section “TfAFM Methodology, Capabilities, and Challenges,” an encounter at instant kT_c is modeled as an impulse input $v_k \delta(t - kT_c)$ to the cantilever, where v_k represents the strength of the impact. It can be assumed that impact strength $v_k = v_k(\bar{a})$ at the k th impact depends on the past m bits. Here, when deciphering a sequence of N bits, the interaction force signal h on the cantilever is given by $h(t) = \sum_{k=0}^{N-1} v_k \delta(t - kT_c)$ with the assumption that

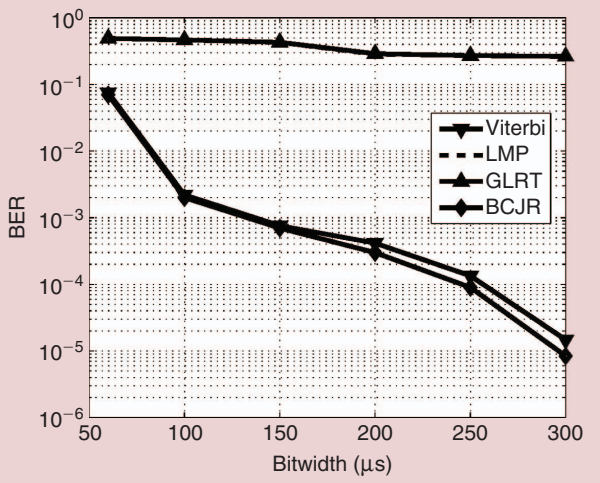


FIGURE 13 A comparison between detectors that incorporate system memory and detectors that do not. Experimental bit error rates (BERs) for Bahl–Cocke–Jelinek–Raviv (BCJR), Viterbi, locally most powerful (LMP), and generalized likelihood ratio test (GLRT) for bit widths varying from 60 to 300 μs . There is a very marginal difference between the LMP and GLRT curves that is not visible in the graph but LMP does perform better than GLRT [25].

$$\bar{v}_i = \bar{\mathfrak{G}}(a_i, a_{i-1}, \dots, a_{i-m}) + \bar{b}_i, \quad (5)$$

where $\bar{\mathfrak{G}}(a_i, a_{i-1}, \dots, a_{i-m})$ is a function of the current and the last m bits and $\bar{v}_i = [\nu_{iq} \nu_{iq+1} \dots \nu_{(i+1)q-1}]^T$, m denotes the system memory, and \bar{b}_i is a zero-mean independent and identically distributed Gaussian vector of length q . The impulsive force input train (with strength ν_k) to the cantilever is processed by the impulse response (given by $\Gamma(t)$) of the error in estimating the deflection using an observer. The output of $\Gamma(t)$ is further corrupted by noise $n(t)$ to result in the innovation error e .

$\bar{\mathfrak{G}}$ and \bar{b}_i capture the dependency of earlier interactions on the present interaction. As shown later, for estimating the source symbol sequence, knowledge of $\bar{\mathfrak{G}}$ and \bar{b}_i is not needed but can be addressed by gathering appropriate statistics in a learning step.

In the context of data storage systems, the detection problem becomes the determination of the source symbols a_i from the innovation signal $e(t)$. It can be shown that the samples of the innovation signal $z_k = e(kT_c)$ form sufficient statistics, and thus determination of the source symbols a_k from the continuous-time innovation signal $e(t)$ can be transformed to the determination of the source-symbol sequence from samples z_k of the innovation signal. A whitening filter is also required if $n(t)$ is colored. Thus after whitening and sampling, the discrete-time signal $z_k = \sum_{k_1=0}^l \nu_{k-k_1}(\bar{a})h_{k_1} + n_k$, where the filter $\{h_k\}_{k=0,1,\dots,l}$ denotes the effect of the whitened matched filter and the sequence $\{n_k\}$ represents the Gaussian noise with variance V (Figure 12).

Accordingly, the maximum likelihood (ML) detection strategy solves the problem

$$\begin{aligned} \hat{a} &= \arg \max_{\bar{a} \in \{0,1\}^N} p(\bar{z} | \bar{a}) \\ &= \arg \max_{\bar{a} \in \{0,1\}^N} \prod_{i=0}^{N-1} p(\bar{z}_i | \bar{a}, \bar{z}_0^{i-1}), \end{aligned} \quad (6)$$

where $\bar{z} = [z_0 z_1 \dots z_{Nq-1}]^T$, \bar{z}_i is the received output vector corresponding to the i th input bit, that is, $\bar{z}_i = [z_{iq} z_{iq+1} \dots z_{(i+1)q-1}]^T$, and $\bar{z}_0^{i-1} = [\bar{z}_0^T \bar{z}_1^T \dots \bar{z}_{i-1}^T]^T$.

The pdf $p(\cdot)$ in (6) is learned from test experiments [25]. Under the assumption that the interactions at the i th bit do not depend beyond $m + m_1$ bits in the past, it can be asserted that

$$p(\bar{z}_i | \bar{a}, \bar{z}_0^{i-1}) \approx p(\bar{z}_i | S_i, S_{i-1}, \bar{z}_{i-m_1}^{i-1}),$$

where the state $S_i = \{a_{i-m-m_1+1}, \dots, a_i\}$ consists of the past $m + m_1$ source symbols. The pdfs $p(\bar{z}_i | S_i, S_{i-1}, \bar{z}_{i-m_1}^{i-1})$ can be estimated from learning experiments where a pseudorandom sequence of source symbols of zeros and ones is first created on the medium and the sampled filtered innovation sequence z_k is measured. From the knowledge of the source symbols and the received z_k , these pdfs can be determined. Further assuming that $p(\bar{z}_{i-m_1}^{i-1} | S_i, S_{i-1})$ is Gaussian with mean $Y(S_i, S_{i-1})$ and covariance $C(S_i, S_{i-1})$, the maximum likelihood problem (6) can be solved using dynamic programming. The solution to the problem yields the optimal source symbol sequence for a received sequence z_k . The above strategy of decoding the source symbol sequence is termed as the *Viterbi decoder scheme*.

Instead of solving the maximum likelihood problem for detecting the entire sequence, a related problem is to obtain the a posteriori probability (APP) of a symbol a_k based on the entire sequence of innovation samples given by \bar{z} defined as $\text{APP}(a_k) = p(a_k | \bar{z})$. In maximum a posteriori symbol detection, the symbol a_k that maximizes the $\text{APP}(a_k)$ is found [26]. In this article, the decoding technique implements the Bahl–Cocke–Jelinek–Raviv (BCJR) algorithm [27].

In the above solution strategies, it is possible to determine measures on the probabilities of making errors (as seen later). Results are presented below that demonstrate the effectiveness of the sequence estimation strategies over other strategies.

In experiments, a cantilever with resonant frequency $f_0 = 71.78$ kHz and quality factor $Q = 67.55$ is oscillated near its resonant frequency. For a given sequence of source symbols $\{a_i\}$, a topographic profile signal $\sum a_k b(t - kT)$ is provided to the cantilever where T is the bit width. In the experimental setup, the bit width can be adjusted from 60 to 350 μs . The bit pattern was generated by a disc piezo, where the dynamics of the piezo were identified by ascertaining its frequency response. A disc piezo is a small piezo actuator with a high-resonance frequency but a small range of travel that sits on the conventional vertical positioning system of an atomic force microscope and is capable of providing high-positioning

bandwidth. An input excitation to the piezo was shaped to obtain the desired bit profile based on the identified model of the piezo. The innovation signal generated by an observer was sampled at the cantilever's resonant frequency f_0 to obtain the sequence $\{z_k\}$. The Viterbi and BCJR decoders require training data to determine the parameters of the assumed model. In the initial training phase of the experiments, a random sequence of bits was generated and the innovations signal were recorded. From the innovations sequence, the matched filter output was determined. The recorded sequence was used to determine locations in the sequence where the various state transitions occur. The corresponding mean vector and covariance matrices of the various transitions were then used to decode the source sequence.

After this training step, parameters in the model were identified. In the evaluation phase, random bits were generated, and both Viterbi detection and the BCJR algorithm were used to detect the bits.

Figure 13 compares results of two classes of detectors: 1) detectors (BCJR and Viterbi) that incorporate the system memory and perform decoding over the entire sequence of source symbols, in which the effect of the past pattern of source symbols on the signature in the innovation signal is learned and incorporated into the decoder, and 2) detectors [generalized likelihood ratio test (GLRT) and locally most powerful (LMP)] that ignore memory effects.

The Viterbi and BCJR decoding produce remarkable results on the experimental data compared to the LMP and the GLRT detectors. Figure 14 provides insights on why the sequence-estimation-based decoders (Viterbi and BCJR) provide better performance. Here the mean vectors for two different source sequences of four bits each, with 300 μ s bit width, are shown. The statistics in Figure 14 are obtained from the learning step where a pseudorandom bit sequence of source symbols $\{a_i\}$ was generated, the corresponding topography signal $a(t)$ with a bit profile $b(t)$ was provided to the topography of the sample, and the innovation signal was measured (see Figure 11). The signatures (as shown in Figure 11) of source-symbol-sequences 1100 and 1101, which only differ in the last bit, are distinct enabling better separation of these sequences and leading to better performance of BCJR and Viterbi detectors. A bit-by-bit detection, as used in GLRT and LMP, does not perform as well, as is evident from the drastically different signatures of, for example, same bit "1" that occur multiple times in the sequences 1100 and 1101.

The measures on the quality of detection can further guide the choice of the bit width, where a longer bit width can be employed to reduce the bit error rate (BER). The Viterbi and BCJR algorithms use a learning step that is essential in estimating the conditional pdfs. Such a learning step is viable in a data storage setting where the bit profile is known and therefore learning can be achieved, for example, by using a pseudorandom sequence of bits written on the medium. Such information is also critical for providing quality measures such as BER on how well the

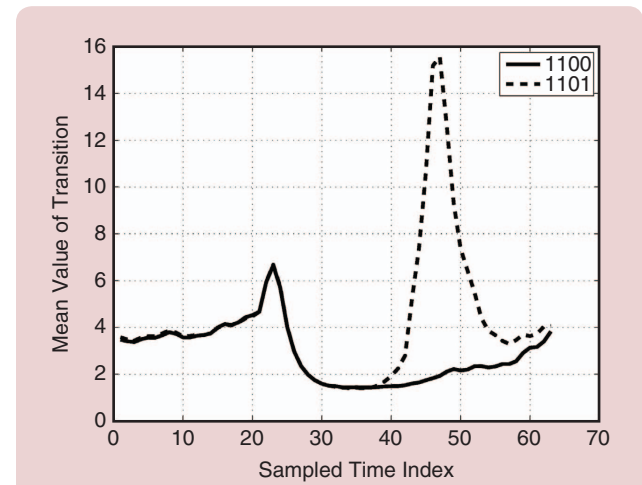


FIGURE 14 Separation of sequences in sequence-based decoders. Mean vector for two state transitions for 300 μ s bit width from experimental data where "1100" and "1101" represents transition from state "110" to state "100" and "101," respectively [25].

information is being decoded. In a more general imaging scenario, the problem is made more difficult, as it is not clear how the learning step is to be achieved. The strategy of improving feature detection by using sequence detection methods, such as the Viterbi and BCJR, instead of a bit-by-bit detection still hold significant promise for further improving and providing measures of the fidelity of imaging and is a focus of current and future research. Some preliminary studies are reported in [26].

An another interesting use of coding theory and sequence detection application is in the use of cantilever probes for sequencing DNA [28].

CONCLUSIONS

This article highlights the necessity of a framework that identifies and corrects for sources of artifacts and provides real-time fidelity measures on inferences from measurements in AFM. The methods developed in this article are preliminary efforts in this direction and pertain mainly to only two specific topography-imaging modes in AFM. The availability of many imaging modes and the versatility of atomic force microscopes with respect to imaging different sample properties evince the magnitude of the task for developing such a framework. The article demonstrates the role of control and communication system-theoretic tools in developing such a framework. Since both control and communication theories have elaborate frameworks to identify, model, and design to mitigate the effects of uncertainties in modeling, they are particularly relevant for identifying artifacts and providing confidence measures in AFM.

AUTHOR INFORMATION

Srinivasa M. Salapaka (salapaka@illinois.edu) received the B.Tech. degree in mechanical engineering from the Indian

Institute of Technology, Madras, in 1995 and the M.S. and Ph.D. degrees in mechanical engineering from the University of California at Santa Barbara, in 1997 and 2002, respectively. During 2002–2004, he was a postdoctoral associate in the Laboratory for Information and Decision Systems, Massachusetts Institute of Technology, Cambridge. Currently, he is an associate professor in the Mechanical Engineering Department at the University of Illinois, Urbana-Champaign. His research interests are nanotechnology, robust control, and classification and aggregation of large data and multi-agent networks. He is a 2005 CAREER award recipient. He can be contacted at 362C, Mechanical Engineering Building, 1206 W Green Street, Urbana, IL 61801 USA.

Aditya Ramamoorthy received the B.Tech. degree in electrical engineering from the Indian Institute of Technology, Delhi, in 1999 and the M.S. and Ph.D. degrees from the University of California, Los Angeles, in 2002 and 2005, respectively. He was a systems engineer at Biomorphic VLSI Inc. until 2001. From 2005 to 2006 he was with the data storage signal processing group at Marvell Semiconductor Inc. Currently, he is an associate professor in the Department of Electrical and Computer Engineering at Iowa State University. His research interests are in the areas of network information theory, channel coding, and signal processing for nanotechnology. He is the recipient of the 2012 Iowa State University's Early Career Engineering Faculty Research Award, the 2012 NSF CAREER award, and the Harpole-Pentair professorship in 2009 and 2010.

Murti V. Salapaka received the B.Tech. degree in mechanical engineering from Indian Institute of Technology, Madras, in 1991 and the M.S. and Ph.D. degrees in mechanical engineering from the University of California at Santa Barbara, in 1993 and 1997, respectively. He was a faculty member in the Department of Electrical and Computer Engineering at Iowa State University from 1997 to 2007. Currently, he is a professor in the Department of Electrical and Computer Engineering at the University of Minnesota, Minneapolis. His research interests are nanotechnology, multiple-objective robust control, and distributed and structural control. He is a 1997 National Science Foundation CAREER Award recipient.

REFERENCES

- [1] G. Binnig, C. F. Quate, and C. Gerber, "Atomic force microscope," *Phys. Rev. Lett.*, vol. 56, no. 9, pp. 930–933, Mar. 1986.
- [2] R. Wisendanger, *Scanning Probe Microscopy and Spectroscopy*. Cambridge, U.K.: Cambridge Univ. Press, 1994.
- [3] G. Haugstad, *Atomic Force Microscopy: Understanding Basic Modes and Advanced Applications*. Hoboken, NJ: Wiley, 2012.
- [4] L. Gross, F. Mohn, N. Moll, P. Liljeroth, and G. Meyer, "The chemical structure of a molecule resolved by atomic force microscopy," *Science*, vol. 325, no. 5944, pp. 1110–1114, 2009.
- [5] S. M. Salapaka and M. V. Salapaka, "Scanning probe microscopy—A control systems perspective on nano-interrogation," *IEEE Control Syst. Mag.*, vol. 28, no. 2, pp. 65–83, 2008.
- [6] T. Ando, N. Kodera, E. Takai, D. Maruyama, K. Saito, and A. Toda, "A high-speed atomic force microscope for studying biological macromolecules," *Proc. Nat. Acad. Sci.*, vol. 98, no. 22, pp. 12468–12472, 2001.
- [7] T. De, P. Agarwal, D. R. Sahoo, and M. V. Salapaka, "Real-time detection of probe loss in atomic force microscopy," *Appl. Phys. Lett.*, vol. 89, no. 13, article 133119, 2006.
- [8] P. Agarwal, T. De, and M. V. Salapaka, "Real time reduction of probe-loss using switching gain controller for high speed atomic force microscopy," *Rev. Sci. Instrum.*, vol. 80, no. 10, pp. 103701–103705, 2009.
- [9] S. Salapaka, A. Sebastian, J. P. Cleveland, and M. V. Salapaka, "High bandwidth nano-positioner: A robust control approach," *Rev. Sci. Instrum.*, vol. 73, no. 9, pp. 3232–3241, 2002.
- [10] A. Sebastian and S. Salapaka, "Design methodologies for robust nanopositioning," *IEEE Trans. Control Syst. Technol.*, vol. 13, no. 6, pp. 868–876, 2005.
- [11] S. Devasia, E. Eleftheriou, and S. O. R. Moheimani, "A survey of control issues in nanopositioning," *IEEE Trans. Control Syst. Technol.*, vol. 15, no. 5, pp. 802–823, Sept. 2007.
- [12] C. Lee and S. M. Salapaka, "Robust broadband nanopositioning: Fundamental trade-offs, analysis, and design in a two-degree-of-freedom control framework," *Nanotechnology*, vol. 20, no. 3, article 035501, 2009.
- [13] B. Bhushan, *Handbook of Micro/Nano Tribology*, 2nd ed. Boca Raton, FL: CRC Press, 1999.
- [14] A. Shegaonkar and S. M. Salapaka, "Feedback based correction of imaging artifacts due to geometrical and mechanical cross-talk and tip-sample stick in atomic force microscopy," *Rev. Sci. Instrum.*, vol. 78, no. 10, article 103706, 2007.
- [15] P. Vettiger, G. Cross, M. Despont, U. Drechsler, U. Durig, B. Gotsmann, W. Haberele, M. A. Lantz, H. Rothuizen, R. Stutz, and G. Binnig, "The millipede—Nanotechnology entering data storage," *IEEE Trans. Nanotechnol.*, vol. 1, no. 1, pp. 39–55, 2002.
- [16] H. Pozidis, W. Haberle, D. W. Wiesmann, U. Drechsler, M. Despont, T. Albrecht, and E. Eleftheriou, "Demonstration of thermomechanical recording at 641 gbit/in²," *IEEE Trans. Magn.*, vol. 40, no. 4, pp. 2531–2536, 2004.
- [17] F. Holzner, P. H. Paul, U. Drechsler, M. Despont, A. W. Knoll, and U. Durig, "High density multi-level recording for archival data preservation," *Appl. Phys. Lett.*, vol. 99, no. 2, article 023110, 2011.
- [18] H. Pozidis, G. Cherubini, A. Pantazi, A. Sebastian, and E. Eleftheriou, "Channel modeling and signal processing for probe storage channels. Selected areas in communications," *IEEE J. Select. Areas Commun.*, vol. 28, no. 2, pp. 143–157, 2010.
- [19] A. Sebastian, M. V. Salapaka, D. Chen, and J. P. Cleveland, "Harmonic balance based analysis for tapping-mode AFM," in *Proc. American Control Conf.*, San Diego, CA, 1999, pp. 232–236.
- [20] A. Sebastian, M. V. Salapaka, D. Chen, and J. P. Cleveland, "Harmonic and power balance tools for tapping-mode atomic force microscope," *J. Appl. Phys.*, vol. 89, no. 11, pp. 6473–6480, June 2001.
- [21] D. R. Sahoo, A. Sebastian, and M. V. Salapaka, "Transient-signal based sample-detection in atomic force microscopy," *Appl. Phys. Lett.*, vol. 83, no. 26, pp. 5521–5523, Dec. 2003.
- [22] D. R. Sahoo, A. Sebastian, and M. V. Salapaka, "Harnessing the transient signals in atomic force microscopy," *Int. J. Robust Nonlinear Control*, vol. 15, no. 16, pp. 805–820, 2005.
- [23] H. V. Poor, *An Introduction to Signal Detection and Estimation*, 2nd ed. New York: Springer-Verlag, 1994.
- [24] D. B. Owen, *Handbook of Statistical Tables*. Reading, MA: Addison-Wesley, 1922.
- [25] N. Kumar, P. Agarwal, A. Ramamoorthy, and M. Salapaka, "Maximum likelihood sequence detector for dynamic mode high density probe storage," *IEEE Trans. Commun.*, vol. 58, no. 6, pp. 1686–1694, June 2010.
- [26] N. Kumar, G. Saraswat, P. Agarwal, A. Ramamoorthy, and M. Salapaka, "High-speed nanoimaging using dynamic mode AFM: A map detection approach," in *Proc. 44th Asilomar Conf. Signals, Systems Computers*, 2010, pp. 1807–1811.
- [27] L. Bahl, J. Cocke, F. Jelinek, and J. Raviv, "Optimal decoding of linear codes for minimizing symbol error rate," *IEEE Trans. Inform. Theory*, vol. 20, no. 2, pp. 284–287, Mar. 1974.
- [28] J. Reed, B. Mishra, B. Pittenger, S. Magonov, J. Troke, M. A. Teitell, and J. K. Gimzewski, "Single molecule transcription profiling with AFM," *Nanotechnology*, vol. 18, no. 4, article 044032, 2007.
- [29] S. Morita, R. Wiesendanger, and E. Meyer, Eds. *Noncontact Atomic Force Microscopy* (NanoScience and Technology). Berlin, Germany: Springer-Verlag, 2002.
- [30] R. Garcia and R. Pérez, "Dynamic atomic force microscopy methods," *Surf. Sci. Rep.*, vol. 47, nos. 6–8, pp. 197–301, 2002.
- [31] Y. Sang, M. Dube, and M. Grant, "Thermal effects on atomic friction," *Phys. Rev. Lett.*, vol. 87, no. 17, article 174301, Oct. 2001.

